Supporting Information

A small-molecule drug inhibits autophagy gene expression through the central regulator TFEB

Yuqi Lin[1†], Qiqi Shi[2†], Guang Yang[3], Fuchun Shi[3], Yang Zhou[4], Tongtong Wang[1], Peng Xu[1,3], Peifeng Li[1], Zaizhou Liu[1], Hanyin Sun[3], Zhixin Zhao[1], Ke Ding[1], Zhen Wang[1], Haizhong Feng[2*], Biao Yu[1,3*], Pengfei Fang[1,3*], Jing Wang[1,3*]

TABLE OF CONTENTS

I. Extended Data Figures and Tables

Supplementary Table S1. Autophagy inhibitors and activators under development.

Compound name	Mode of action and target(s)	Status	Key reference(s)
Autophagy inhibitors			
SAR405	VPS34	In preclinical development	(1)
VPS34-IN1	VPS34	In preclinical development	(2)
Autophinib	VPS34	In preclinical development	(3)
Azaquindole-1	VPS34	In preclinical development	(4)
ULK-101	ULK1	In preclinical development	(5)
SBI-0206965	ULK1	In preclinical development	(6)
Compound 19a	ATG14L	In preclinical development	(7)
FMK-9a	ATG4B	In preclinical development	(8)
Compound 19b	ATG7	In preclinical development	(9)
Autogramin-2	GRAMD1A/Aster-A	In preclinical development	(10)
ML-SI3	TRPML1 inhibitor	In preclinical development	(11)
TCH-165	20S proteasome activator	In preclinical development	(12)
Bafilomycin A1	v-ATPase	Experimental agent	(13)
Concanamycin	v-ATPase	In preclinical development	(14)
Salicylihalamide A	v-ATPase	In preclinical development	(15)
Lobatamide	v-ATPase	In preclinical development	(16)
Diphyllin	v-ATPase	In preclinical development	(17)
VE (cyclodepsipeptide verucopeptin)	v-ATPase	In preclinical development	(18)
BRD1240	v-ATPase	In preclinical development	(19)
Chloroquine and hydroxychloroquine	Lysosomotropic	Extensively used in the past as an antimalarial agent	(20)
Oxautin-1	Lysosomotropic	In preclinical development	(21)
Autoquin	Lysosomotropic	In preclinical development	(22)
3-methyladenine (3-MA)	VPS34 inhibition	Experimental agent	(23)
Azithromycin	Unknown	Approved for treatment of multiple bacterial infections	(24)
Cardiac glycosides	Na^+ /K^+ -ATPase inhibition	Extensively used in the past for treatment of cardiac disorders	(25)
Compound C (also known as dorsomorphin)	AMPK inhibition	In preclinical development	(26)
Edavarone	ROS scavenger	Experimental agent	(27)
LY294002	VPS34 inhibition	In clinical trials for the treatment of refractory neuroblastoma	(28)
Lys05	Lysosomal inhibition	In preclinical development	(29)
Mdivi-1	Mitophagy inhibition	In preclinical development	(30)
Melatonin	Altered ROS production	In clinical trials for treatment of a wide panel of conditions	(31)
MRT67307	ULK1 inhibition	In preclinical development	(32)
MRT68921	ULK1 inhibition	In preclinical development	(32)
NSC185058	ATG4B inhibition	In preclinical development	(33)
Wortmannin	VPS34 inhibition	Experimental agent	(34)
Autophagy activators			
Rapamycin	FKBP12/mTORC1	Approved for use in coronary stents (to prevent transplant rejection) and to treat a rare pulmonary disease	(35, 36)
Torin-1	mTORC1	Experimental agents	(37)

AZD8055	mTORC1	In clinical trials for the treatment of advanced solid malignancies or lymphomas	(38)
EN6	v-ATPase activation	In preclinical development	(39)
OSW-1	oxysterol-binding protein (OSBP)	In preclinical development	(40)
BRD1991	Bcl-2	In preclinical development	(41)
MK6-83	TRPML1 activation	In preclinical development	(42)
Tat-beclin-1	GAPR-1	In preclinical development	(43)
SMER-28	Unknown	In preclinical development	(44)
Carbamazepine	Sodium voltage-gated channel (SCN5A)	Approved for treatment of seizures and bipolar disorders	(45)
Felodipine	L-type calcium channel	Approved for treatment of hypertension (high blood pressure)	(46)
FT-385	USP30	In preclinical development	(47)
A-769662	AMPK activation?	In preclinical development	(48)
Antimycobacterial antibiotics	Altered ROS production	Approved for treatment of mycobacterial infections	(49)
BECN1-derived peptide	BECN1 activator	In preclinical development	(50)
BRD5631	Unknown	In preclinical development	(51)
Caloric restriction	Multiple	NA (not applicable)	(52)
Carbon monoxide	Altered ROS production	Experimental agent	(53)
Chloramphenicol	Unknown	Approved for second-line treatment of bacterial infections	(54)
Everolimus (also known as RAD-001)	mTORC1 inhibition	Approved for cancer therapy	(55)
Hydrogen sulfide	AMPK activation?	Experimental agent	(56)
Hydroxycitrate	CRM (caloric restriction mimetic)	Clinically tested for treatment of diabetes, now discontinued	(57)
IFNγ	MAPK activation?	In clinical trials, mainly for cancer immunotherapy	(58)
Lithium	Reduction in Ins(1,4,5)P_3 and inositol levels	Approved for treatment of bipolar disorders	(59)
Melatonin	Altered ROS production	In clinical trials for the treatment of a wide range of conditions	(60)
Metformin	AMPK activation?	Approved for treatment of type 2 diabetes	(61)
Physical exercise	Multiple	NA (not applicable)	(62)
Resveratrol	CRM (caloric restriction mimetic)	Nutritional supplement that is available over the counter; in clinical trials for treatment of several disorders	(63)
Retinoic acid	Unknown	Approved for cancer therapy (all-trans-retinoic acid, ATRA)	(64)
Simvastatin	AMPK activation?	Approved for treatment of obesity	(34)
Spermidine	CRM (caloric restriction mimetic)	Nutritional supplement that is available over the counter	(65)
Temsirolimus (also known as CCI-779)	mTORC1 inhibition	Approved for cancer therapy	(66)
Trehalose	Unknown	In clinical trials for treatment of bipolar disorders, dry eye syndrome and vascular ageing	(67)
Trichostatin A	Unknown	Discontinued from clinical tests	(23)
Vorinostat	Unknown	Approved for cancer therapy	(68)

Supplementary Table S2. Crystallographic statistics

	TFEB_HLHLZ
Data collection	
Space group	*P3₁21*
Cell dimensions	
a, *b*, *c* (Å)	54.60, 54.60, 185.30
α, β, γ (°)	90.00, 90.00, 120.00
Resolution (Å)	47.28–2.00 (2.05–2.00)*
CC(1/2)	1.000 (0.918)
I / s*I*	27.2 (2.1)
Completeness (%)	99.2 (100.0)
Redundancy	18.6 (19.7)
Refinement	
No. reflections	22280
R_{work} / R_{free} (%)	22.2/23.8
R.m.s. deviations	
Bond lengths (Å)	0.005
Bond angles (°)	0.790
Ramachandran plot	
Most favored [%]	98.54
Additional allowed [%]	1.46

Statistics for the highest-resolution shell are shown in parentheses.

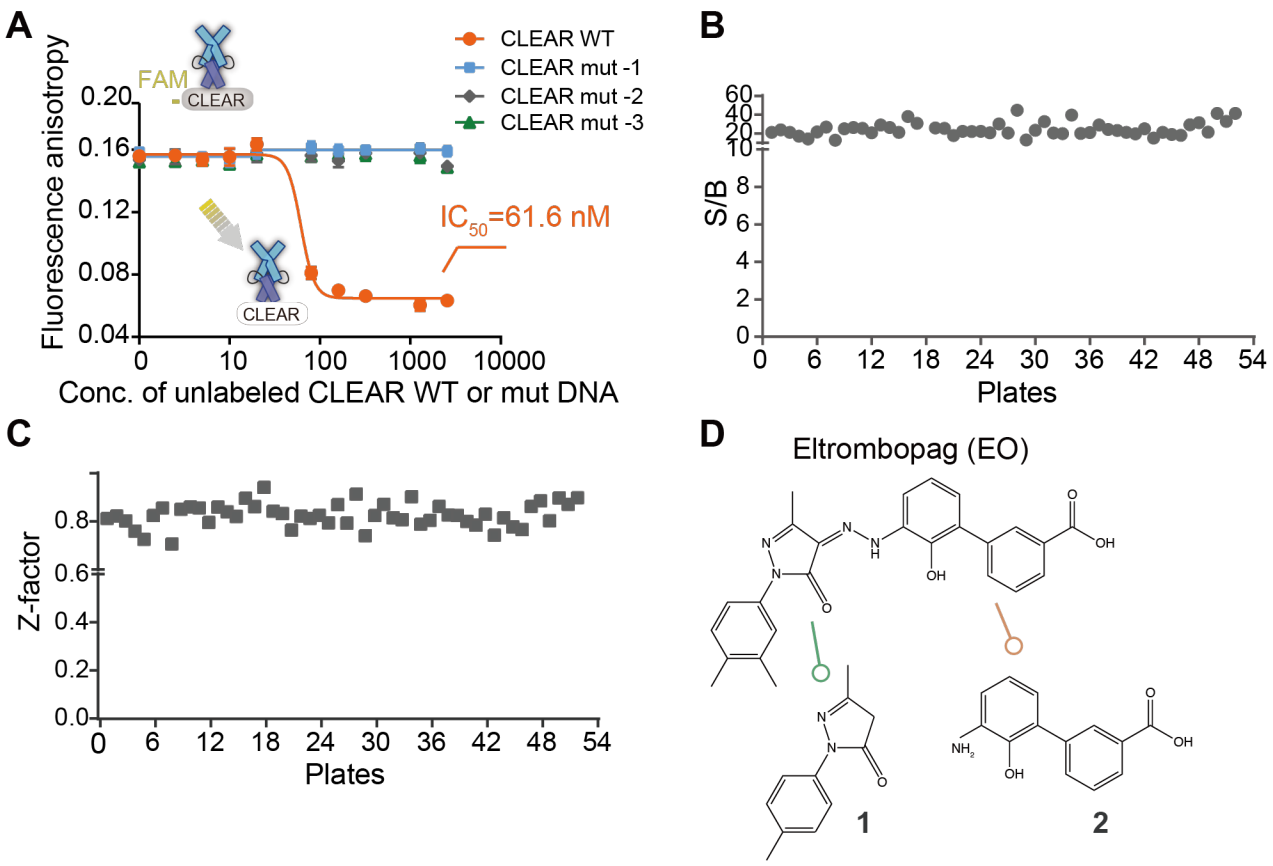

Figure S1. Fluorescence anisotropy-based compound screening to explore TFEB inhibitors.

(A) Serial diluted unlabeled CLEAR DNA or unlabeled mutant CLEAR DNAs (CLEAR mut -1, -2, -3) were titrated to a solution containing 80 nM MBP-TFEB and 10 nM $_{FAM}$-CLEAR-DNA, and the fluorescence anisotropy was measured. Unlabeled CLEAR DNA competitively bound TFEB and released $_{FAM}$-CLEAR DNA, thus reducing fluorescence anisotropy. Unlabeled mutant CLEAR DNAs could not bind TFEB, thus had no effect on the fluorescence anisotropy of $_{FAM}$-CLEAR-DNA. Error bars represent the SDs of four repeats.

(B) The whole screening assay had a stable signal-to-background (S/B) ratio (~25.41 ± 9.09).

(C) The Z'-factors in the screening experiment was also very stable (~0.83 ± 0.049).

(D) Chemical structures of Eltrombopag (EO), and two substructures of EO, compound **1** (3-methyl-1-p-tolyl-5-pyrazolone) and **2** (3'-amino-2'-hydroxy-[1,1'-biphenyl]-3-carboxylic acid).

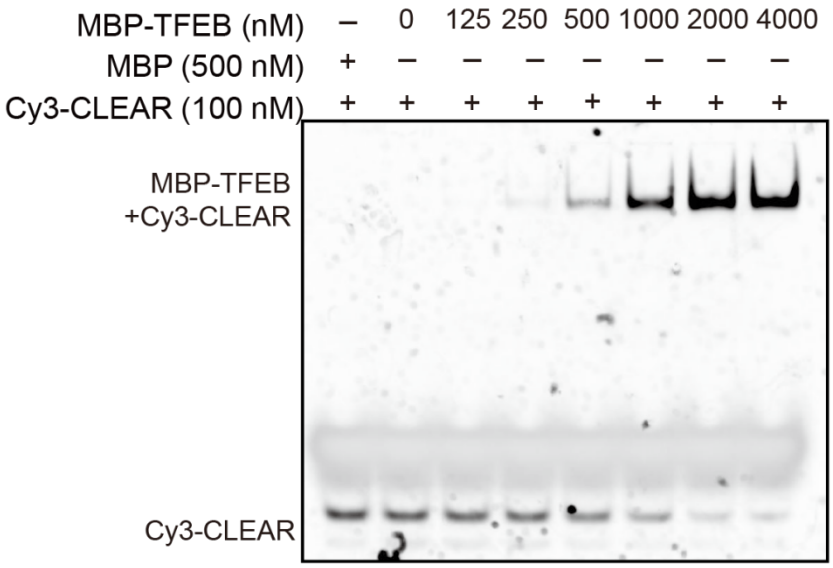

Figure S2. Electrophoretic mobility shift assay (EMSA) showing that binding MBP-TFEB (maltose-binding protein tagged TFEB) significantly slowed the migration of Cy3 labeled CLEAR DNA ($_{Cy3}$.CLEAR) in a dose-dependent manner.

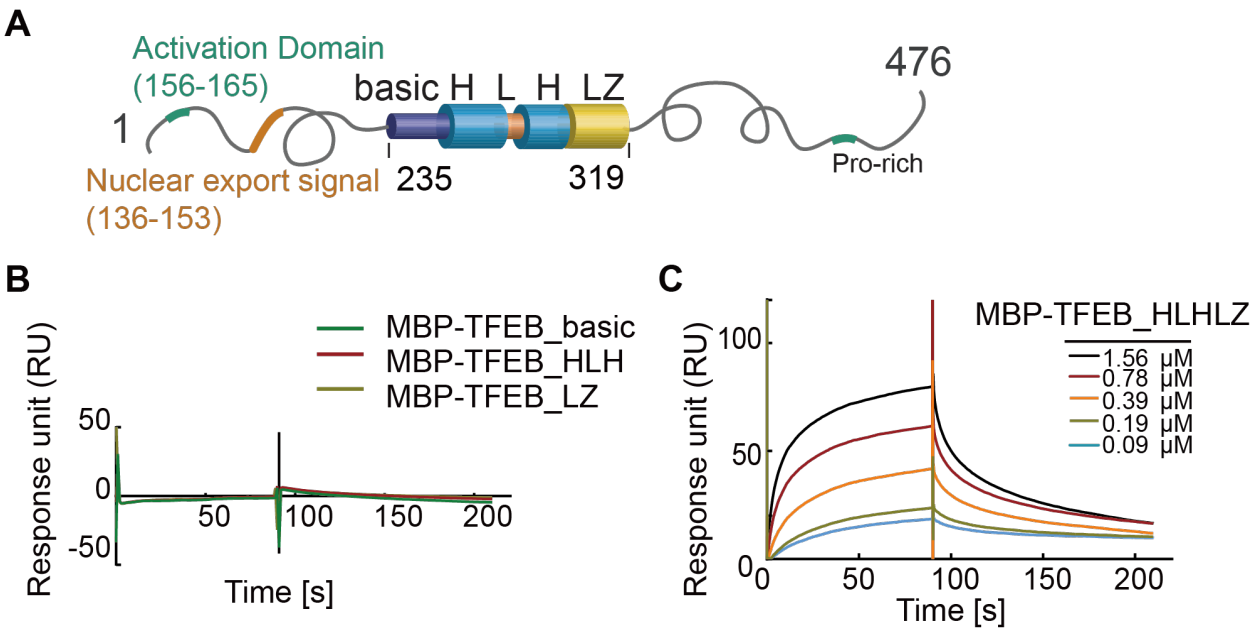

Figure S3. EO binds HLH-LZ region, but not the basic region of TFEB.

(A) Domain scheme of human TFEB isoform 1 protein.

(B) EO-Biotin was immobilized on a SA chip, and its interaction with MBP tagged basic region, HLH region and LZ region of TFEB were analyzed with surface plasmon resonance (SPR) experiments. The concentration of each tested protein was 300 nM and no binding signal was detected.

(C) EO-Biotin was immobilized on a SA chip, and its interaction with MBP tagged HLH-LZ region of TFEB was analyzed with SPR experiment. The kinetic parameters are k_{on} = 3.56E4±7.00E2 $(M \cdot s)^{-1}$, k_{off} = 1.08E-2±1.20E-4 s^{-1}, and Kd = 304.0 nM.

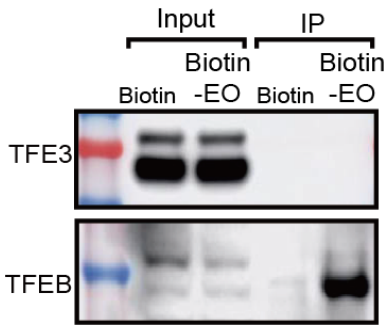

Figure S4. Pulldown–western blot experiment showing that Biotin-EO interacted with the endogenous TFEB but not with TFE3 in U87 cell lysate.

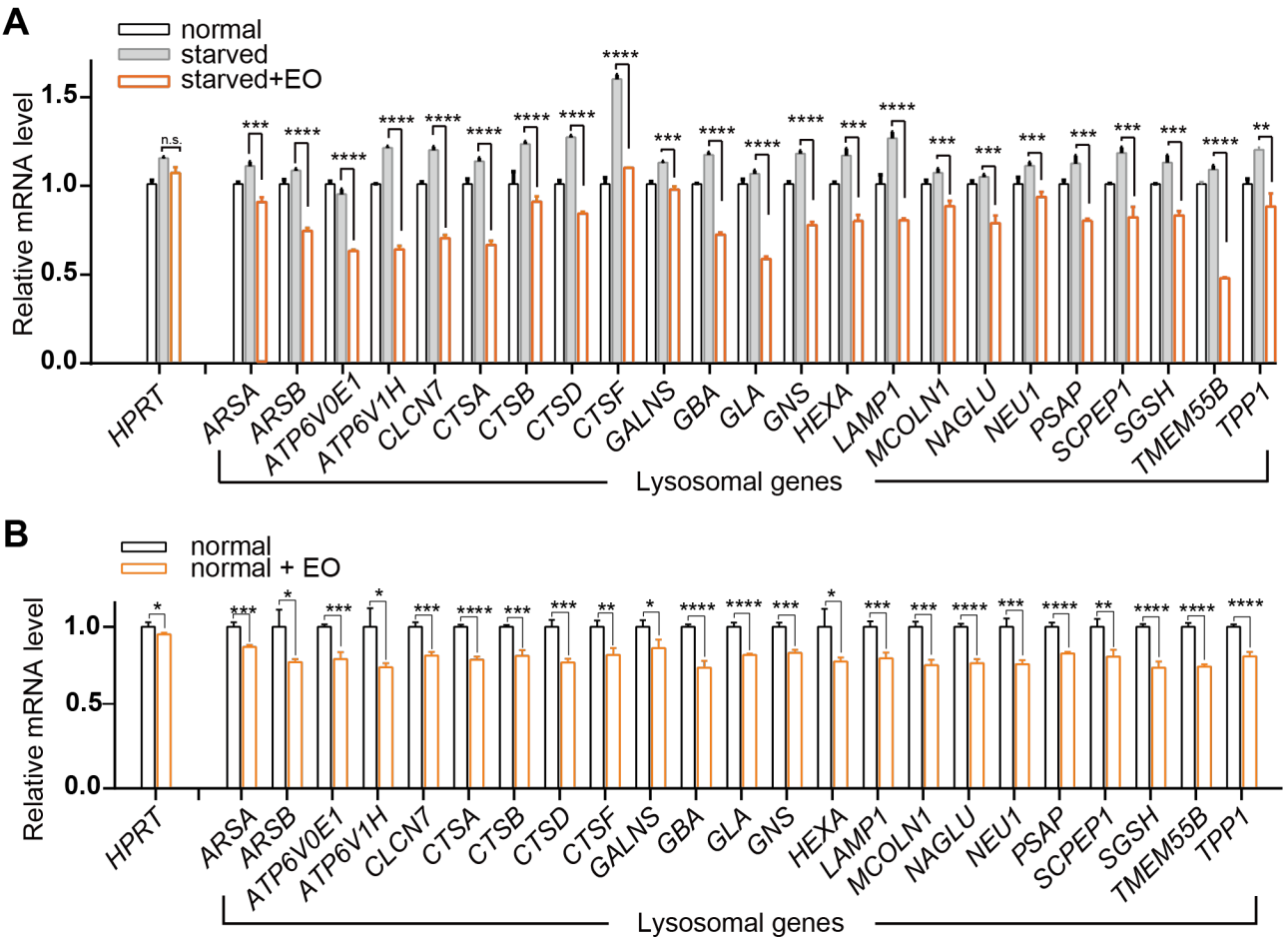

Figure S5. EO inhibits TFEB transcriptional activity under normal condition or HBSS-starvation.

(A) Reverse transcription-polymerase chain reaction (RT-PCR) analysis of the mRNA level of lysosomal genes in HeLa cells treated with normal medium, nutrient-deprived HBSS medium with or without EO (5 μM). The mRNA levels were normalized relative to *GAPDH*. Error bars represent the SDs of three repeats. Student's *t* test (unpaired); *P* ** <0.01; *P* *** <0.001; *P* **** <0.0001 and no significant (n.s.).

(B) RT-PCR analysis of the mRNA level of lysosomal genes in HeLa cells cultured in normal medium with or without EO (5 μM). The mRNA levels were normalized relative to *GAPDH*. Error bars represent the SDs of four repeats. Student's *t* test (unpaired); *P* * <0.05; *P* ** <0.01; *P* *** <0.001; *P* **** <0.0001.

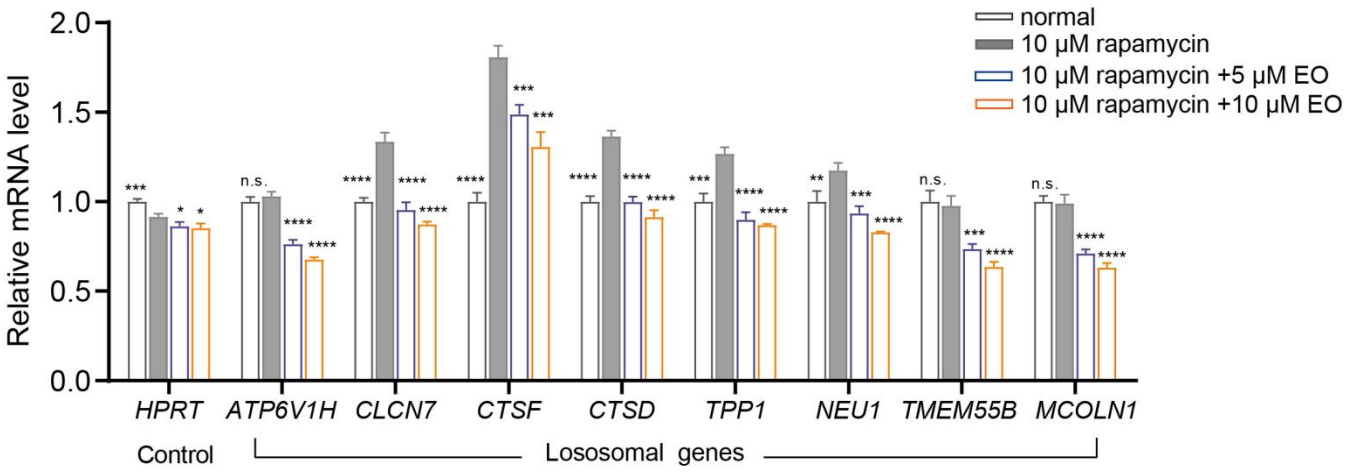

Figure S6. EO inhibits the TFEB transcriptional activation upon rapamycin treatment. RT-PCR analysis of the mRNA levels of lysosomal genes from HeLa cells treated with DMSO, or 10 μM rapamycin with or without EO (concentration as indicated) for 14 h. The mRNA levels were normalized relative to *GAPDH*. *HPRT* is a representative housekeeping control gene. Error bars represent the SDs of four repeats. Significance relative to the 10 μM rapamycin group were calculated with Student's t test (unpaired); *P* * <0.05; *P* ** <0.01; *P* *** <0.001; *P* **** <0.0001.

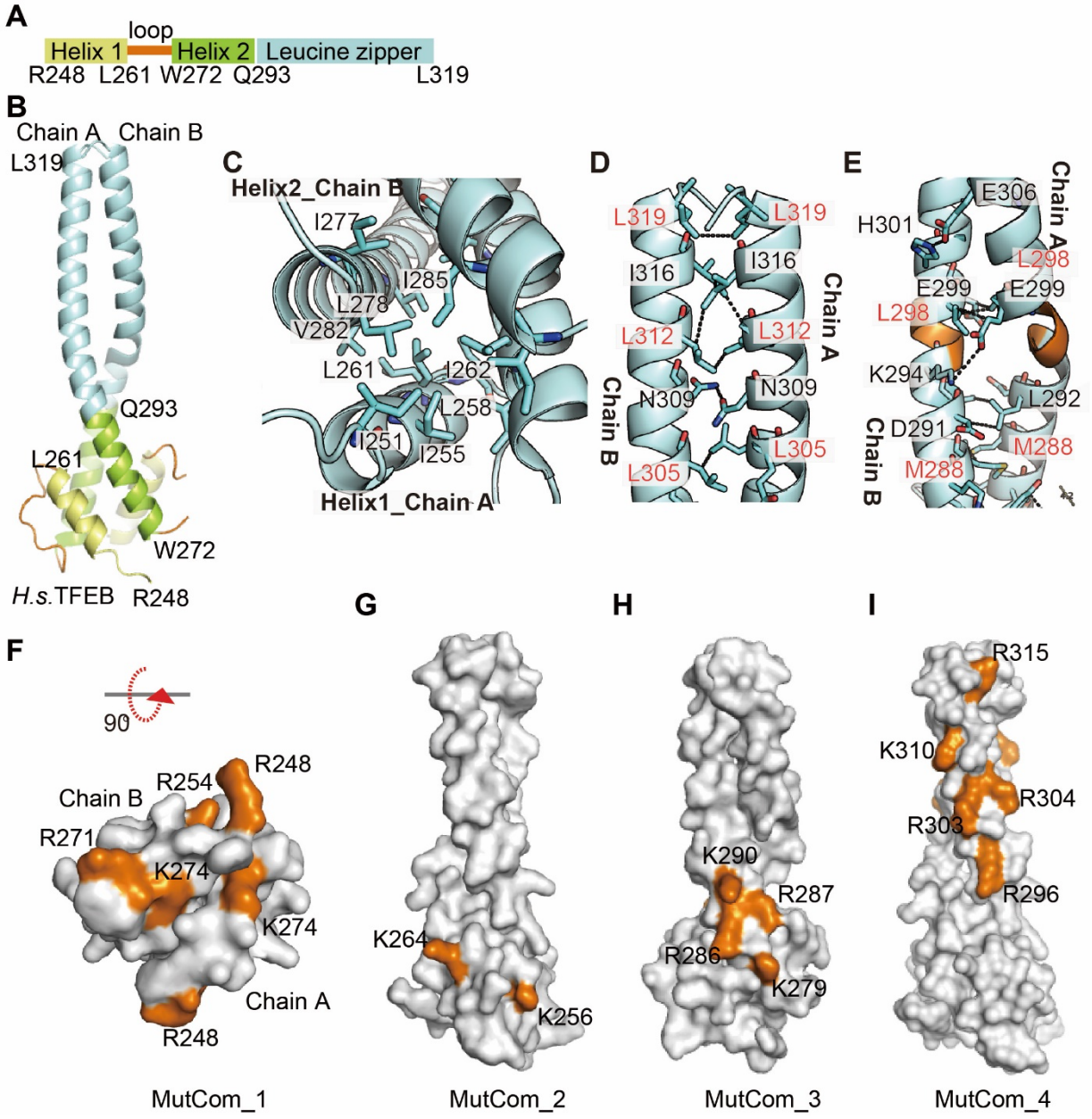

Figure S7. Crystal structure of TFEB.

(**A**) Domain scheme of the crystallized Helix1-Loop-Helix2-Leucine zipper region of human TFEB ($TFEB_{HLH-LZ}$).

(**B**) Overall crystal structure the $TFEB_{HLH-LZ}$. It contains two crystallographically independent molecules, chain A and chain B, to form a compact dimer.

(C) A hydrophobic four-helix bundle was constituted by residues on Helix 1 (including I255, L258, L261 and I262) and residues on Helix 2 (including I277, L278, V282 and I285) from both chain A and chain B.

(D) The typical heptad repeats of leucine residues, including L298, L305, L312, and L319, mediate the dimerization of TFEB.

(E) Residues I316, N309, H301, E306, L292, K294, and E299 on LZ from both chains form additional hydrophobic interactions or H-bonds that further facilitate the dimer formation of TFEB.

(F-I) Distribution of residues tested in alanine scanning mutagenesis. In MutCom_1, R248, R254, R271 and K274 on the bottom surface of HLH region were mutated to alanine **(F)**; In MutCom_2, K256 and K264 on the side surface of HLH region were mutated to alanine **(G)**; In MutCom_3, K279A, R286A, R287A, and K290A on the side surface of HLH region were mutated to alanine **(H)**; In MutCom_4, R296, R303, R304, K310 and R315 on the leucine zipper were mutated to alanine **(I)**.

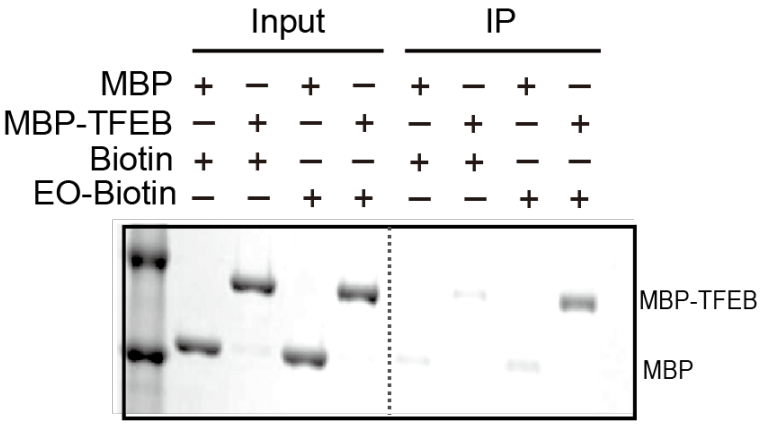

Figure S8. Pulldown assay monitoring the interaction between EO and TFEB. EO-Biotin or Biotin control was used to pulldown MBP-TFEB, and MBP control. Proteins were analyzed by Coomassie Blue staining.

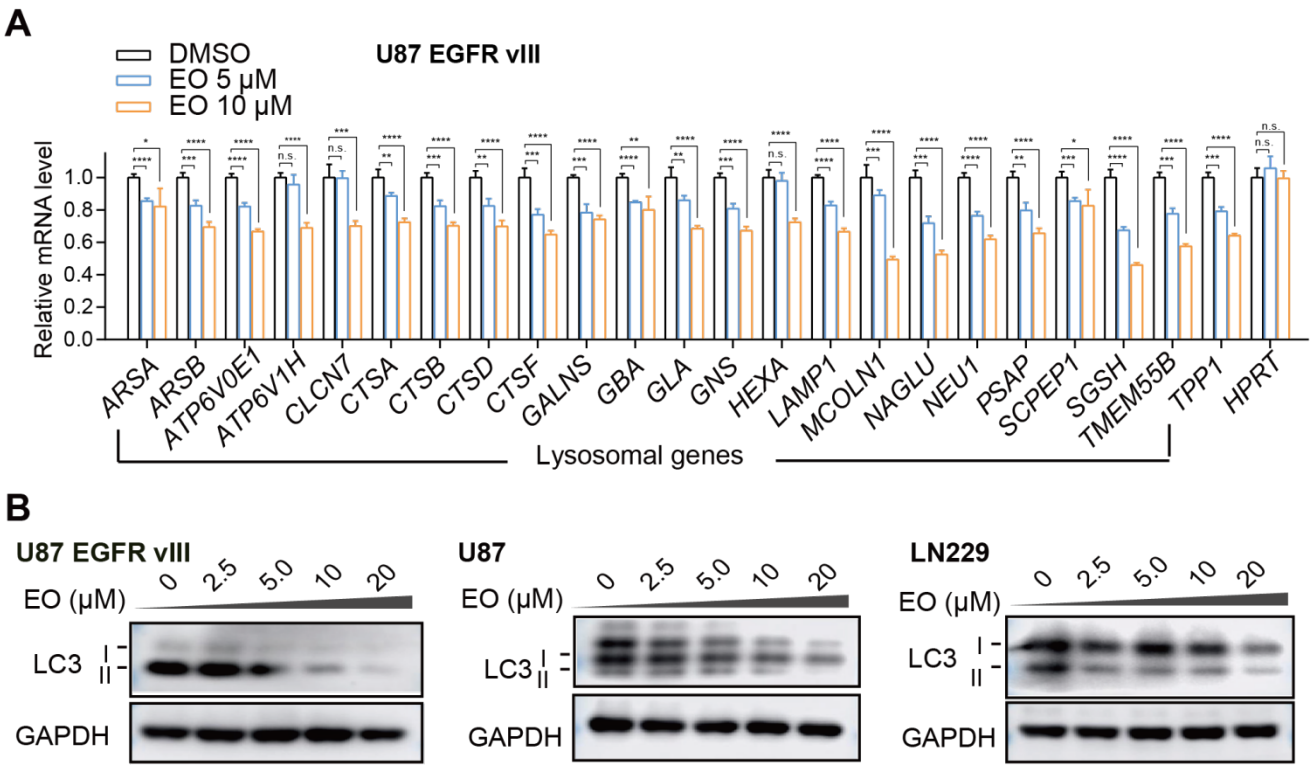

Figure S9. EO decreases the lysosomal genes expression and LC3-II formation in glioblastoma cells.

(A) RT-PCR analysis of lysosomal genes expression in glioblastoma cells U87 EGFR vIII after treatment of DMSO control or EO with indicated concentrations. *HPRT* is a housekeeping gene, and others are lysosomal genes. The mRNA levels were normalized relative to *GAPDH*. Error bars represent SDs of four repeats. Student's *t* test (unpaired); *P* * <0.05; *P* ** <0.01; *P* *** <0.001; *P* **** <0.0001 and no significant (n.s.).

(B) EO attenuates LC3-II formation in multiple glioblastoma cell lines. The cells were treated with EO at indicated concentrations and then LC3-II was measured by western blotting. GAPDH was used as a loading control.

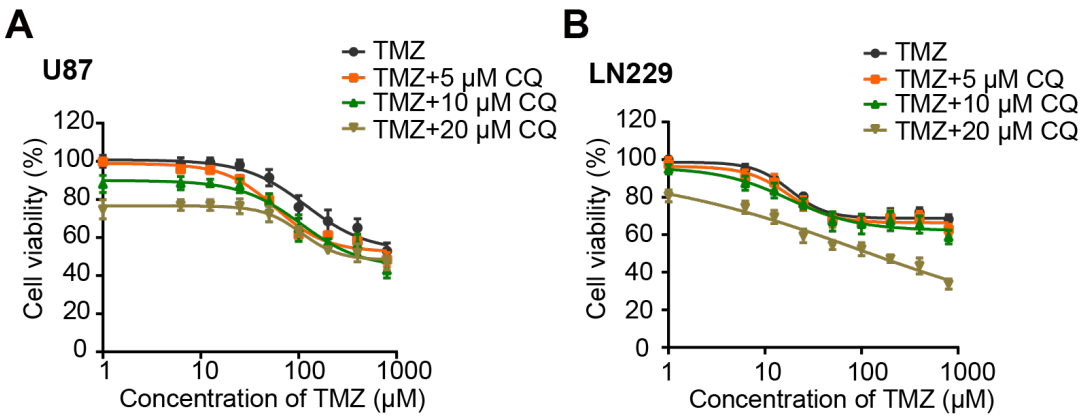

Figure S10. Cytotoxicity of Chloroquine (CQ) in combination with temozolomide (TMZ) on glioblastoma cells U87 (A) and LN229 (B). The cell viabilities were assessed with the cell counting kit-8 (CCK-8) assay and normalized relative to untreated control samples. Error bars represent SDs of five repeats.

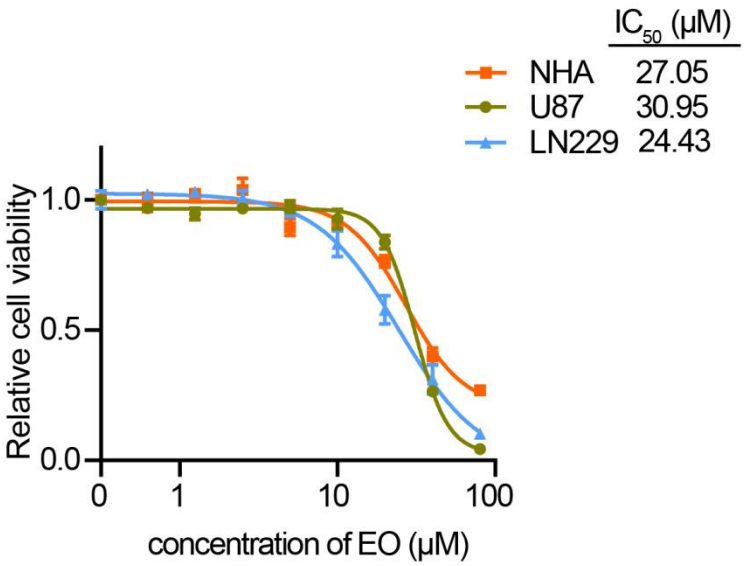

Figure S11. Cytotoxicity of EO on glioblastoma cells U87 and LN229, as well as the non-cancerous cells NHA of same origin. The cell viabilities were assessed with the Cell-TiterGlo luminescent assay and normalized relative to untreated control samples. Error bars represent SDs of three repeats.

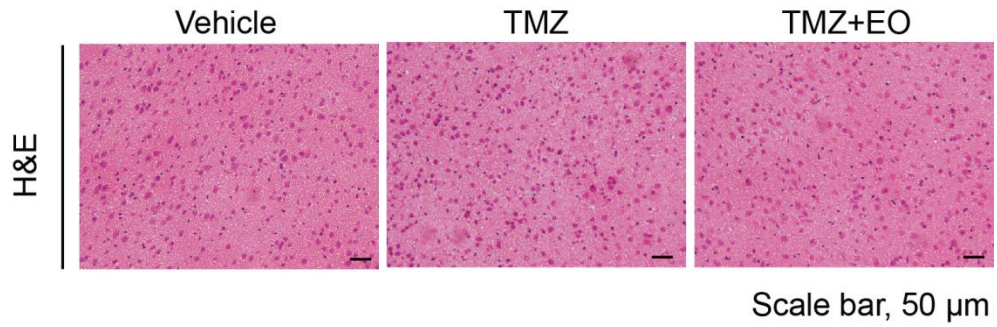

Figure S12. Representative images of hematoxylin and eosin (H&E) on the other half normal brain sections from mice bearing orthotopic tumors treated with TMZ, TMZ+EO, or vehicle.

II. Materials and Methods of Chemical Synthesis

Commercial sources of key compounds

The FDA-approved drug library used for compound screening was purchased from Selleck Chemicals (catlog no. L1300). Compound Eltrombopag (EO) was purchased from Shanghai Titan Scientific Co.,Ltd. (catlog no. 01140648). Compounds **1** (3-Methyl-1-p-tolyl-5-pyrazolone, catlog no. BD13080) and **2** (3'-Amino-2'-hydroxy-[1,1'-biphenyl]-3-carboxylic acid, catlog no. BD83791) were purchased from Bide Pharmatech Ltd.

Chemical synthesis of biotinylated Eltrombopag (EO-Biotin)

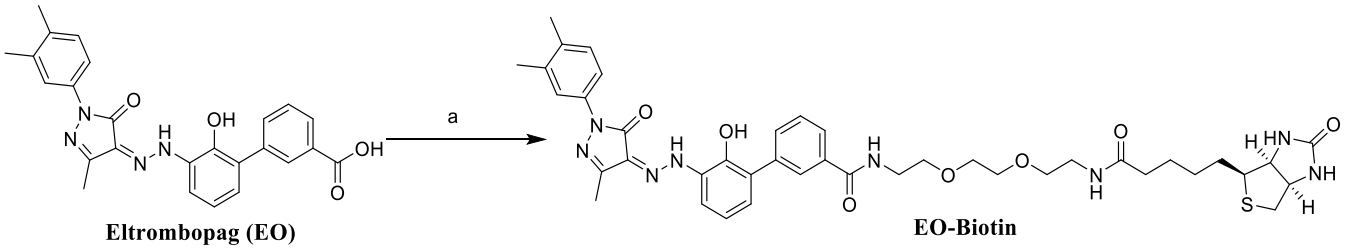

Reagents and conditions: a. Biotin-PEG_2-NH_2, EDCI, HOBT, THF, RT, 70%.

Procedure: To a mixture of (Z)-3'-(2-(1-(3,4-dimethylphenyl)-3-methyl-5-oxo-1,5-dihydro-4H-pyrazol-4-ylidene)hydrazinyl)-2'-hydroxy-[1,1'-biphenyl]-3-carboxylic acid (**EO**) (20.0 mg, 0.045 mmol) and Biotin-PEG2-NH2 (16.8 mg, 0.045mmol) in THF (2.0 mL) was added EDCI (12.8 mg, 0.068 mmol) and HOBT (0.9 mg, 0.0068mmol), the reaction mixture was stirred for 6 h at room temperature. The mixture was concentrated in vacuo, the residue was purified by silica gel chromatography to afford **EO-Biotin** (25.1 mg, 70%): ^{1}H NMR (500 MHz, Methanol-d_4) δ 8.01 (s, 1H), 7.89 – 7.82 (m, 1H), 7.79 – 7.69 (m, 2H), 7.67 (s, 1H), 7.58 (d, *J* = 8.0 Hz, 2H), 7.14 (dd, *J* = 21.0, 10.3 Hz, 3H), 4.47 – 4.39 (m, 1H), 4.23 (dq, *J* = 6.9, 2.3 Hz, 1H), 3.72 – 3.56 (m, 8H), 3.53 (t, *J* = 5.4 Hz, 2H), 3.13 (s, 1H), 2.86 (d, *J* = 12.1 Hz, 1H), 2.66 (d, *J* = 12.5 Hz, 1H), 2.44 (s, 1H), 2.37 (s, 3H), 2.30 (s, 3H), 2.26 (s, 3H), 2.13 (dd, *J* = 13.8, 6.0 Hz, 2H), 1.67 – 1.45 (m, 5H), 1.41 – 1.33 (m, 2H). MS (ESI) *m/z* 799.3 $[M + H]^+$, 821.3 $[M + Na]^+$.

Chemical synthesis of compound 3

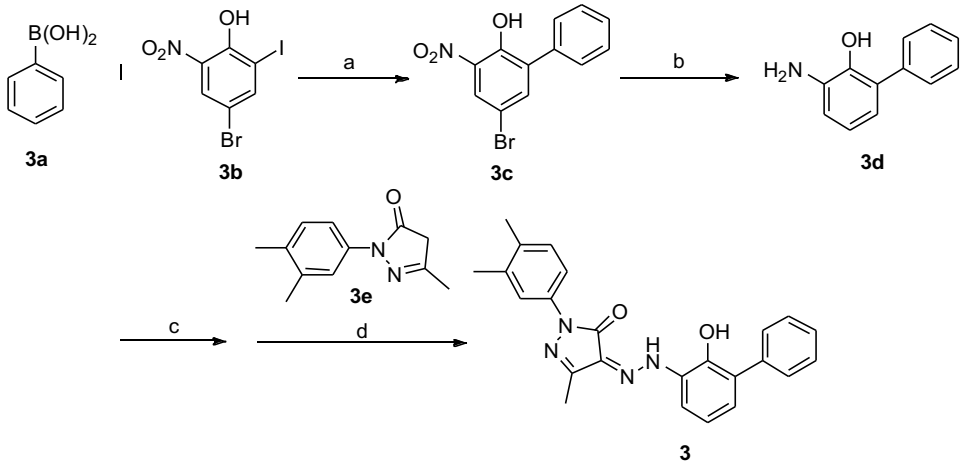

Reagents and conditions: a) Na_2CO_3, $Pd(OAc)_2$, acetone, H_2O, Ar, reflux, 25%; b) H_2, NaOH, Pd/C, triethylamine, 50 °C, 57%; c) $NaNO_2$, MeOH, HCl (aq), 0 °C, sulfamic acid; d, $NaHCO_3$ (aq), 79% (two steps).
Procedures:

5-bromo-3-nitro-[1,1'-biphenyl]-2-ol (3c). To a flask charged with a magnetic bar were added **3a** (1.0 g, 8.2 mmol), **3b** (1.0 g, 8.2 mmol), Na_2CO_3 (1.8 g, 17 mmol) and $Pd(OAc)_2$ (30 mg, 0.14 mmol) followed by addition 15 mL acetone and 15 mL water under Ar atmosphere. The mixture was heated to 90 °C and stirred until the reaction finished. The reaction mixture was partitioned between 20 mL saturated NH_4Cl (aq) and 40 mL dichloromethane. The aqueous was extracted with dichloromethane (40 mL × 2) and the combined organic layer was washed with brine, dried over Na_2SO_4, filtered, concentrated under low pressure and purified by column chromatography to afford 500mg red oil product (500 mg, 1.7 mmol, 25% yield). ^{1}H NMR (400 MHz, Chloroform-d) δ 11.03 (s, 1H), 8.27 (s, 1H), 7.74 (s, 1H), 7.57 – 7.40 (m, 5H). MS (ESI) *m/z* 292.1, 293.9 $[M - H]^-$.

3-amino-[1,1'-biphenyl]-2-ol (3d). To a solution of **3c** (500 mg, 1.7 mmol) in 20 mL MeOH was added triethylamine (396mg, 3.9 mmol) dropwise followed by the addition of PdC (60mg, 0.57 mmol). The reaction mixture was stirred at 30 °C under hydrogen atmosphere overnight. After the reaction finished, Pd/C was filtered and the filtrate was concentrated and purified by column chromatography to afford 180 mg red solid product (180 mg, 0.97 mmol, 57% yield). ^{1}H NMR (500 MHz, Chloroform-d) δ 7.55 – 7.38 (m, 5H), 6.84 (t, *J* = 7.7 Hz, 1H), 6.75 (dd, *J* = 7.9, 1.6 Hz, 1H), 6.70 (dd, *J* = 7.5, 1.6 Hz, 1H). MS (ESI) *m/z* 186.3 $[M + H]^+$.

(Z)-2-(3,4-dimethylphenyl)-4-(2-(2-hydroxy-[1,1'-biphenyl]-3-yl)hydrazineylidene)-5-methyl-2,4-dihydro-3H-pyrazol-3-one (3). **3d** (58 mg, 0.31 mmol) was dissolved in 5 mL MeOH at 0 °C followed by addition of 1.0 g 4 M HCl (aq) with vigorous stirring. Then $NaNO_2$ (19 mg, 0.28 mmol) dissolved in 2 mL water was added dropwise to the mixture and the reaction was allowed to stir for 1 h at 0 °C. Subsequently, sulfamic acid (5 mg, 0.05 mmol) was added to the mixture followed by stirring for another 1 h. With the diazo salt obtained in suit, $NaHCO_3$ (aq) as the pH regulator was added to adjust the pH value into 7~8 with the addition of **3e** to the mixture. The reaction underwent the slow raise of temperature from 0 °C to r. t. and stirred overnight. 4 M HCl (aq) was added to adjust the pH value into 5 and followed by precipitation of massive solid in the mixture. The solid was filtered and washed with 4 M HCl (aq) and MeOH, then dried to afford **3** as a red solid (78 mg, 0.20 mmol, 79% yield). ^{1}H NMR (500 MHz, Chloroform-d) δ 7.72 (d, *J* = 2.2 Hz, 1H), 7.66 (dd, *J* = 8.2, 2.3 Hz, 1H), 7.54 – 7.46 (m, 5H), 7.43 (q, *J* = 4.4 Hz, 1H), 7.16 (d, *J* = 8.3 Hz, 1H), 7.11 (dd, *J* = 7.6, 1.6 Hz, 1H), 7.05 (t, *J* = 7.8 Hz, 1H), 2.35 (s, 3H), 2.30 (s, 3H), 2.26 (s, 3H). ^{13}C NMR (126 MHz, Chloroform-d) δ 157.79, 147.71, 142.84, 137.35, 136.33, 135.91, 133.75, 130.03, 129.96, 129.35, 129.13, 128.65, 128.34, 128.31, 127.17, 121.30, 119.93, 116.35, 115.50, 20.13, 19.47, 11.96. HRMS (ESI) for $C_{24}H_{23}N_4O_2$ $[M + H]^+$, calcd: 399.1816, found: 399.1818.

III. Experimental Procedures of Biological Experiments

Protein preparation

The maltose-binding protein (MBP) tagged TFEB constructs, including MBP-TFEB (containing the bHLH-LZ domain of human TFEB isoform 1, residues 230-319), MBP-TFEB_basic (containing the basic region, residues 230–248), MBP-TFEB_HLH (containing the helix-loop-helix region, residues 249–291), MBP-TFEB_LZ (containing the leucine zipper region, residues 288–319), MBP-TFEB_HLH-LZ (containing the helix-loop-helix-leucine zipper region, residues 248–319), were generated with the pHis-MBP-TEV vector. TFEB mutants MutCom_1, MutCom_2, MutCom_3, MutCom_4, R248A, R254A, R271A and K274A were constructed based on MBP-TFEB. All the plasmids were induced to be expressed in the bacterial strain Rosetta with 0.2 mM isopropylthio-galactoside (IPTG) at 16 °C for 20 h, and purified to homogeneity with a Ni-HiTrap affinity column and a size exclusion S200 column (GE Healthcare).

To obtain the HLH-LZ domain of TFEB, the His-MBP tag was removed by TEV protease form purified MBP-TFEB_HLH-LZ, and the cleaved protein was passed through a HiTrap MBP column followed by purifications with a HiTrap SP Sepharose column and a size exclusion S75 column (GE Healthcare).

Fluorescence anisotropy assay

Fluorescence anisotropy measurements were carried out using an EnVision® Multimode Plate Reader (PerkinElmer). $_{FAM}$-CLEAR DNA (5'-FAM-AGGTCACGTGACCGG-3', final concentration 10 nM) was mixed with gradient MBP-TFEB or MBP control (0–2560 nM) in a buffer containing 20 mM HEPES pH 7.5, 200 mM NaCl, 1 mM $MgCl_2$, and 2.5% (v/v) glycerol. The measurement was performed after 2 h of incubation at 4 °C. For competition assay, unlabeled CLEAR DNA (5′-AGGTCACGTGACCGG-3′) or unlabeled mutant CLEAR DNAs (CLEAR mut-1: 5′-AGGTCTGCAGACCGG-3′; CLEAR mut-2: 5′-AGGTTCCGTGACCGG-3′; CLEAR mut-3: 5′-AGGTTCCGGAACCGG-3′) (0–2560 nM) were pre-incubated with MBP-TFEB (final concentration 80 nM) in buffer containing 20 mM HEPES pH 7.5, 200 mM NaCl, 1 mM $MgCl_2$, 2.5% (v/v) glycerol for 12 h at 4 °C. $_{FAM}$-CLEAR DNA was then added to the mixtures with final concentration of 10 nM. The measurement was performed after 2 h of incubation. Because the experiment used perfectly complementary double-stranded DNA, the sequence of one DNA strand is shown.

To detect the IC_{50} of eltrombopag, **1**, **2, 3** and EO-Biotin to disrupt MBP-TFEB and $_{FAM}$-CLEAR DNA interaction, MBP-TFEB (final concentration 50 nM) was mixed with eltrombopag, **1**, **2, 3** and EO-Biotin (0–10000 nM) in buffer containing 20 mM HEPES pH 7.5, 200 mM NaCl, 1 mM $MgCl_2$, 2.5% (v/v) glycerol and incubated for 12 h at 4 °C. $_{FAM}$-CLEAR DNA was then added to the mixtures with final concentration of 5 nM. The measurement was performed after 2 h of incubation.

An excitation beam at 480 nm and emission at 535 nm were used to detect the fluorescence anisotropy. The binding affinity Kd was calculated using the equation with receptor depletion:

$$A = A_{\mathrm{f}} + (A_{\mathrm{b}} - A_{\mathrm{f}}) \times \frac{(\mathrm{L_T} + \mathrm{K_d} + \mathrm{R_T}) - \sqrt{(\mathrm{L_T} + \mathrm{K_d} + \mathrm{R_T})^2 - 4\mathrm{L_T}\mathrm{R_T}}}{2\mathrm{L_T}}$$

L_T = the total added concentration of ligand; A = the experimental anisotropy; A_f = the anisotropy for the free ligand; A_b = the anisotropy for the fully bound ligand.

Electrophoretic mobility shift assay (EMSA)

CLEAR DNA (5′-GTA GGT CAC GTG ACC GGG-3′) was labeled with fluorophore Cy3 (denoted as $_{Cy3}$-CLEAR) at the 5' end. Serial diluted MBP-TFEB (0-4 μM), or 500 nM MBP control was incubated with 100 nM $_{Cy3}$-CLEAR in buffer containing 10 mM Tris pH 8.0, 50 mM KCl, 1 mM DTT, 2 mM $MgCl_2$ and 5% (v/v) glycerol at 4° for 2 h. The resulting DNA–protein complex and free DNA were separated by a 6% non-denaturing polyacrylamide gel. The gel was photographed with Amersham™ Imager 600 (GE Healthcare) under fluorescence detection mode with stimulation light 520 nm and Cy3 filter.

To assess the effect of EO to disrupt TFEB-CLEAR DNA complex, MBP-TFEB (final concentration of 500 nM) was incubated with serial diluted EO (0–12.5 μM) in buffer containing 10 mM Tris pH 8.0, 50 mM KCl, 1 mM DTT, 2 mM $MgCl_2$ and 5% (v/v) glycerol at 4°C for 12 h. Then, the Cy3-CLEAR DNA was added to the mixtures with final concentration of 100 nM, and incubated at 4°C for 2 h before electrophoresis.

Surface plasmon resonance (SPR) assay

The binding affinity between EO and TFEB was measured using a Biocore T200 (GE Healthcare). Biotin conjugated EO (EO-Biotin) was immobilized at a level of 167 resonance units on a SA chip (GE Healthcare). MBP control, MBP-TFEB_bHLH-LZ, MBP-TFEB_basic, MBP-TFEB_HLH, MBP-TFEB_LZ, and MBP-TFEB_HLH-LZ in PBS binding buffer (pH 7.4) were injected to flow through the chip at a rate of 30 $\mu L \cdot min^{-1}$ respectively. Sensorgrams were fitted to a simple 1:1 Langmuir interaction model (A+B⇌AB) using the Biocore T200 Evaluation Software analysis program.

Chromatin immunoprecipitation (ChIP) assay

HeLa cells that transiently expressing 3×FLAG human TFEB (isoform 1, residues 1–476) were cultured in above mentioned normal culture medium (DMEM supplemented with 10% FBS and 1% Penicillin-Streptomycin) (normal), or in normal medium supplemented with 10 μM EO (pre-dissolved in DMSO) for 12 h then in Earle's Balanced Salt Solution (EBSS) plus 10 μM EO for 1h (starved + EO), or in normal medium supplemented with relevant concentration of DMSO for 12 h then in EBSS with same concentration of DMSO for 1h (starved), respectively. The cells were rinsed twice with PBS, and the medium was replaced with FBS-free DMEM or EBSS. The cells were crosslinked with 1% formaldehyde (Sangon Biotech, E672001-0100) for 15 min at room temperature, and the reaction was stopped by adding glycine to a final concentration of 125 mM for 5 min at room temperature. Fixed cells were rinsed twice with ice-cold PBS. The Nuclear and Cytoplasmic Protein Extraction kit (Beyotime Institute of Biotechnology, P0028) was used for nucleocytoplasmic isolation. Nucleus was resuspended in radio immunoprecipitation assay (RIPA) buffer containing 50 mM Tris pH 7.4, 150 mM NaCl, 1% NP-40, 0.1% SDS, protease inhibitor cocktail (Bimake, B14001), and sonicated for 15 min (5 sec on/10 sec off) to shear DNA to an average fragment size of 200-1000 bp. The sample was centrifuged at 20,000 ×g for 5 min. The supernatant was used immediately in ChIP experiments. The sonicated chromatin was incubated with anti-FLAG magnetic beads

(Sigma, M8823) at 4 °C overnight on a vertical roller. The beads were washed for 5 minutes, once in low salt buffer containing 0.1% SDS, 1% Triton X-100, 2 mM EDTA pH 8, 20 mM Tris-HCl pH 8 and 150 mM NaCl, twice in high salt buffer containing 0.1% SDS, 1% Triton X-100, 2 mM EDTA pH 8, 20 mM Tris-HCl pH 8 and 500 mM NaCl, twice in LiCl buffer containing 0.25 M LiCl, 1% NP-40, 1% sodium deoxycholate, 1 mM EDTA pH 8 and 10 mM Tris-HCl pH 8, and once in PBS. After the precipitated material was eluted from anti-FLAG magnetic beads, chromatin was reverse-crosslinked by adding 0.2 M NaCl and Proteinase K (Sangon Biotech, B600169-0600), and incubated at 65 °C overnight. DNA levels were quantified by real-time PCR using primers as previous described (69).

Pulldown assay

To assess the interaction between EO and endogenous TFEB or TFE3, 50 μL streptavidin-coated magnetic beads (Thermo scientific, 88816) was saturated in 300 μL solution of 100 μM D-biotin (negative control, BBI Life Sciences, A100340-0001) or 100 μM EO-Biotin (dilute in PBS + 10% DMSO) at 4°C for 1h. Then the beads were washed with 300 μL PBS for four times. 1 mL U87 cell lysate ($1x10^7$ cells) in radio immunoprecipitation assay (RIPA) buffer containing 50 mM Tris-HCl pH 7.4, 150 mM NaCl, 1% NP-40, 0.1% SDS, protease inhibitor cocktail (Bimake, B14001) and phosphatase inhibitors cocktail (Bimake, B15002) was added to the D-biotin or EO-Biotin pre-treated beads and oscillated at 4°C for 2h. For unlabeled EO competition assay, 1 mL U87 cell lysate ($1x10^7$ cells) in radio immunoprecipitation assay (RIPA) buffer was pre-incubated with 1% DMSO (control), 175 μM EO or 350 μM EO overnight, then incubated with the D-biotin or EO-Biotin pre-treated beads and oscillated at 4°C for 2h. The cell lysate was removed and the beads were washed with PBS for three times. The bead bound protein was eluted and denatured with 40 μL loading buffer containing 100 mM Tris-HCl pH 6.8, 4% SDS, 20% (v/v) glycerol, 5% β-mercaptoethanol, 0.004% (w/v) bromophenol blue and boiled at 100 °C for 10 min. Finally, the samples were subjected to SDS-PAGE electrophoresis and analyzed by Western Blot.

To assess the interaction between EO and TFEB WT, TFEB mutants including MutCom_1, MutCom_2, MutCom_3, MutCom_4, R248A, R254A, R271A and K274A, 50 μL streptavidin-coated magnetic beads (Thermo scientific, 88816) was saturated in 300 μL solution of 10 μM EO-Biotin (dilute in PBS + 10% DMSO) at 4°C for 1h. Then the beads were washed with 300 μL PBS for four times. 100 μg purified TFEB WT, TFEB mutant as indicated, and MBP control in buffer containing 20 mM HEPES pH 7.5, 250 mM NaCl, 0.8% BSA was then added to beads and incubated with shaking at 4 °C for 2 h. The protein solution was removed and the beads were washed with wash buffer containing 20 mM HEPES pH 7.5, 250 mM NaCl, 0.5% NP-40, 0.1% BSA for three times. The bead bound protein was eluted and denatured with 100 μL loading buffer containing 100 mM Tris-HCl pH 6.8, 4% SDS, 20% (v/v) glycerol, 5% β-mercaptoethanol, 0.004% (w/v) bromophenol blue and boiled at 100 °C for 10 min. Finally, the samples were subjected to SDS-PAGE electrophoresis and analyzed by Western Blot.

Equal amounts of protein from the total cell lysates, or pull down fractions were separated by SDS-PAGE (8–16% gradient gel), and transferred to nitrocellulose membrane or PVDF membrane using wet transfer. The membranes were blocked in 5% BSA (SIGMA, V900933) or 5% milk (Sangon Biotech, A600669-0250) for 1–2 h, and probed overnight at 4 °C with primary antibodies diluted in 5% BSA (SIGMA, V900933) in 1X TBST buffer. The

following antibodies were used: GAPDH (Proteintech, 60004-1-Ig), FLAG (Proteintech, 20543-1-AP), TFEB (Invitrogen, PA5-21616), and TFE3 (abcam, ab93808). Then, the membranes were washed with TBST and probed with the respective secondary isotype-specific antibodies (BBI Life Sciences, D110087-0100, D110058-0100). Then the membranes were washed with TBST and analyzed using the LumiBest ECL reagent solution kit (Share-Bio, sb-wb011 or sb-wb012).

Reverse-transcription PCR assay

The cells were cultured in normal culture medium (DMEM supplemented with 10% FBS and 1% Penicillin-Streptomycin), or in normal medium supplemented with 0.1% DMSO, indicated concentrations of EO (pre-dissolved in DMSO) for 12 h then starved in EBSS or HBSS supplemented with the same concentrations of DMSO and EO for 4 h. To detect the effect of EO treatment on TFEB's transcriptional activity under basal autophagy (without starving), HeLa cells were cultured in normal culture medium supplemented with 0.1% DMSO (normal) or 5 μM EO (normal + 5 μM EO) for 14 h. To detect the effect of EO treatment on TFEB's transcriptional activity in glioblastoma cells, LN229, U87 or U87-EGFRvIII were treated with 0.1% DMSO, 5 μM EO or 10 μM EO for 12 h. To detect the effect of EO on the mRNA levels of TFEB target lysosomal genes which was activated by rapamycin treatment. HeLa cells were treated with 0.1% DMSO or 10 μM rapamycin with gradient concentrations of EO (0, 5 μM or 10 μM) for 14 h. Total RNA was extracted using PureLink™ RNA Mini Kit (Invitrogen, 12183018A), according to the manufacturer's instructions. Quality and quantity of RNA was determined by Nanodrop (DeNovix, DS-11 Spectrophotometer). Reverse transcription was performed using HiScript® II Q RT SuperMix for qPCR (+gDNA wiper) (Vazyme, R223-01). Real-time quantitative PCR (qRT-PCR) was performed using AceQ® qPCR SYBR Green Master Mix (Vazyme, Q111-02) or ChamQ™ SYBR® qPCR Green Master Mix (Vazyme, Q331-02). The relative levels of expression of genes were normalized relative to an internal control (*GAPDH*).

Nuclear and cytoplasmic protein extraction

HeLa cells that transiently expressing 3×FLAG human TFEB (isoform 1, residues 1–476) were cultured in normal culture medium (DMEM supplemented with 10% FBS and 1% Penicillin-Streptomycin) supplemented with 0.1% DMSO (normal) or 10 μM EO (normal + EO) for 14 h, or in normal medium supplemented with 0.1% DMSO or 10 μM EO for 12 h then in Earle's Balanced Salt Solution (EBSS) plus 0.1% DMSO (starved) or 10 μM EO (starved + EO) for 2h, respectively. Then the extraction and isolation of nuclear and cytoplasmic protein were performed according to the instructions for the Nuclear and Cytoplasmic Protein Extraction Kit (Beyotime, P0028). Equal amounts of protein were separated by SDS-PAGE (8–16% gradient gel), and transferred to nitrocellulose membrane using wet transfer. The membranes were blocked in 5% milk (Sangon Biotech, A600669-0250) for 1 h 30 min, and probed overnight at 4 °C with primary antibodies diluted in 5% BSA (SIGMA, V900933) in 1X TBST buffer. The following antibodies were used: FLAG (Proteintech, 20543-1-AP), GAPDH (Proteintech, 60004-1-Ig), Histone H3 (Proteintech, 17168-1-AP). Then, the membranes were washed with TBST and probed with the respective secondary isotype-specific antibodies (BBI Life Sciences, D110087-0100, D110058-0100). Then the membranes were washed with TBST and analyzed using the LumiBest ECL reagent solution kit (Share-Bio, sb-wb011 or sb-wb012).

RNA Sequencing (RNA-Seq) analysis

HeLa cells were cultured in normal culture medium (DMEM supplemented with 10% FBS and 1% Penicillin-Streptomycin), or in normal medium supplemented with 0.1% DMSO, or 10 μM EO for 12 h then starved in EBSS supplemented with the same concentrations of DMSO and EO for 4 h. Total RNA was isolated using PureLink™ RNA Mini Kit (Invitrogen, 12183018A). The sequencing was done by the Annaroad Gene Technology Co., Ltd. A total amount of 2 μg RNA per sample was used as input material for the RNA sample preparations. Sequencing libraries were generated using NEBNext® Ultra™ RNA Library Prep Kit for Illumina® (#E7530L, NEB, USA) following the manufacturer's recommendations and index codes were added to attribute sequences to each sample. Briefly, mRNA was purified from total RNA using poly-T oligo-attached magnetic beads. Fragmentation was carried out using divalent cations under elevated temperature in NEBNext First Strand Synthesis Reaction Buffer (5X). First strand cDNA was synthesized using random hexamer primer and RNase H. Second strand cDNA synthesis was subsequently performed using buffer, dNTPs, DNA polymerase I and Rnase H. The library fragments were purified with QiaQuick PCR kits and elution with EB buffer, then terminal repair, A-tailing and adapter added were implemented. The aimed products were retrieved and PCR was performed. The clustering of the index-coded samples was performed on a cBot cluster generation system using HiSeq PE Cluster Kit v4-cBot-HS (Illumina) according to the manufacturer's instructions. After cluster generation, the libraries were sequenced on an Illumina platform and 150 bp paired-end reads were generated.

Detection of LC3, p62 and TFEB

To detect the effect of EO on the formation of LC3-II and p62 during starvation, HeLa cells were cultured in normal culture medium (DMEM supplemented with 10% FBS and 1% Penicillin-Streptomycin), or in normal medium supplemented with 0.1% DMSO, indicated concentrations of EO for 12 h then starved in EBSS with the same concentrations of DMSO or EO for 2 h. To detect the effect of EO on the formation of LC3-II in glioblastoma cells, LN229, U87 or U87-EGFRvIII were treated with 0.1% DMSO, indicated concentrations of EO for 24 h. To detect the protein state of TFEB, HeLa cells that transiently expressing 3×FLAG human TFEB (isoform 1, residues 1–476) were cultured in normal culture medium (normal), or in normal medium supplemented with 0.1% DMSO or 10 μM EO for 12 h then in Earle's Balanced Salt Solution (EBSS) plus 0.1% DMSO (starve) or 10 μM EO (starve + EO) for 1h, respectively. Whole cell protein extracts (protein lysates) were prepared using laemmli lysis buffer (0.125 M Tris pH 6.8, 4% SDS, 20% (v/v) glycerol, 5% β-mercaptoethanol, 0.004% (w/v) bromophenol blue) supplemented with protease inhibitor cocktail (Bimake, B14001) and phosphatase inhibitors cocktail (Bimake, B15002).

Equal amounts of protein from the total cell lysates were separated by SDS-PAGE (8–16% gradient gel), and transferred to nitrocellulose membrane or PVDF membrane using wet transfer. The membranes were blocked in 5% BSA (SIGMA, V900933) or 5% milk (Sangon Biotech, A600669-0250) for 1 - 2 h, and probed overnight at 4 °C with primary antibodies diluted in 5% BSA (SIGMA, V900933) in 1X TBST buffer. The following antibodies were used: LC3B (Novus Biologicals, NB100-2220), GAPDH (Proteintech, 60004-1-Ig), SQSTM1/p62 (Cell Signaling Technology, #5114), FLAG (Proteintech, 20543-1-AP). Then, the membranes were washed with TBST and probed with the respective secondary isotype-specific antibodies (BBI Life Sciences, D110087-0100, D110058-0100). Then the membranes were washed with TBST and analyzed using the LumiBest ECL reagent solution kit (Share-Bio, sb-wb011 or sb-wb012).

Flow cytometry

HeLa cells were seeded into 24-well plates at a density of 40000 cells per well. Cells were cultured in normal culture medium (DMEM supplemented with 10% FBS and 1% Penicillin-Streptomycin), or in normal medium supplemented with 0.1% DMSO, or 10 μM EO for 12 h then starved in EBSS supplemented with the same concentrations of DMSO and EO for 2 h. Then cells were collected and treated using Guava® Autophagy LC3 Antibody-based Assay Kit. CQ (chloroquine, 100 μM) was added to the system according to manufacturer's instructions to prevent the lysosomal degradation of LC3 and prolong the experimental signal. Data were collected on a flow cytometer system (Guava EasyCyte™ 8HT) and were analyzed with FlowJo software. FITC fluorescence was collected from at least 5000 cells per sample.

Confocal microscopy

HeLa cells stably expressing GFP-LC3-(ATG4 cleavage site)-RFP were grown on glass coverslips for 24 h. Cells cultured in normal culture medium (DMEM supplemented with 10% FBS and 1% Penicillin-Streptomycin), or in normal medium supplemented with 0.1% DMSO, or 10 μM EO for 12 h then starved in EBSS supplemented with the same concentrations of DMSO and EO for 2 h. Cells were washed with PBS and fixed with 4% paraformaldehyde at room temperature for 15 min. DAPI (4’ ,6-diamidino-2-phenylindole, Invitrogen) staining was used to detect the nucleus. Coverslips were mounted on glass slides and the fixed cells were imaged on a laser scanning microscope (Leica-microsystems, Leica-SP8).

Cell viability assay of EO treatment

Cells were seeded in triplicates onto 96-well plates at a density of 3000–5000 per well and then treated with EO at the indicated concentrations for 72 hours. Cell viability was analyzed with Cell-TiterGlo luminescent assay (Promega, G7570) according to the manufacturer’s instructions. Briefly, CellTiter-Glo reagent was added to each well and incubated at room temperature for 10 minutes. The luminescent signals were measured by GloMax Discover Microplate Reader (Promega). The cell viabilities were normalized to average viability of control wells.

Drug synergy assay

Cell Counting Kit-8 (CCK-8) assays were used to assess the viability of different cell lines after treatment of serial diluted compound. After 72 h of incubation, 10 μL Cell Counting Kit-8 (CCK-8, APExBIO, K1018) was added to each well at the end of incubation. The cells were then incubated for another 4 h at 37 °C. The absorbance of each well at 450 nm was read by a EnVision® Multimode Plate Reader (PerkinElmer). The drug synergy assay was performed to assess the cell viability after treatment with EO (0, 5, 10, and 20 μM) in combination with gradient temozolomide (TMZ, 0–800 μM). The drug synergy scores were based on the Bliss model and were determined using website: https://synergyfinder.fimm.fi/ (70).

Crystallization, data collection, and structure refinement

Crystallization of TFEB_HLH-LZ was performed by the sitting-drop vapor-diffusion method at 18 °C for 5 days. The crystallization drop was prepared by mixing 0.5 μL of the protein solution (20 $mg \cdot mL^{-1}$) with 0.5 μL of precipitant

solution containing 0.12 M Ethylene glycols, 0.1 M Buffer system 3, and 50% Precipitant Mix 2 (from Morpheus, Molecular Dimensions).

The crystal mounted in a loop was soaked briefly in a cryoprotectant solution consisting of the corresponding reservoir solution supplemented with 7% (v/v) glycerol and was then flash-frozen in liquid nitrogen. X-ray diffraction data were collected on beamline 19U1 at the Shanghai Synchrotron Radiation Facility (SSRF) using a PILATUS detector (71). All frames were collected at 100 K using a 0.5 oscillation angle with an exposure time of 0.2 s per frame. The crystal-to-detector distance was set to 400 mm. The images were processed with the XDS package using the XDSgui interface (72). The structure was solved by the molecular replacement using the program Molrep (73). Iterative model building and refinement were performed using Coot and Phenix (74, 75).

Docking calculations and molecular dynamics

Structures of the TFEB protein was prepared using the Protein Preparation Wizard (Schrödinger, LLC, New York, NY, 2021) and the missing loops were added using Prime. The prepared structure was equilibrated for 500 ns in molecular dynamics (MD) simulations using Desmond. The MD trajectory frames were clustered and SiteMap was applied to identify the binding sites. The grids for Glide docking were then generated using the receptor grid generation tools, which used an enclosing box of 20 Å around the site identified by SiteMap with other settings left as default. Glide docking with Extra Precision (XP) was used for docking scoring. The top scored binding poses were subjected to MD simulations to examine the stability. The OPLS4 force field was used and the SPC solvent model used to solvate the system. The system was relaxed before simulation using default setting and simulated in the NPT ensemble with the temperature at 300 K and the pressure set at 1 atm.

IV. Abbreviations

TFEB	transcription factor EB
MITF	microphthalmia-associated transcription factor
TFE3	transcription factor E3
bHLH-LZ	basic helix-loop-helix leucine zipper
HLH-LZ	helix-loop-helix leucine zipper
HLH	helix-loop-helix
LZ	leucine zipper
MBP	maltose-binding protein
MBP-TFEB	maltose-binding protein tagged TFEB
CLEAR	coordinated lysosomal expression and regulation
EO	eltrombopag
EO-Biotin	biotin-labeled eltrombopag
TMZ	temozolomide
CQ	chloroquine
HCQ	hydroxychloroquine
BafA1	Bafilomycin A1
LC3	microtubule-associated protein 1A/1B light chain 3
SQSTM1/p62	sequestosome 1 (SQSTM1, also known as p62 protein)
EBSS	earle's balanced salt solution
HBSS	hank's balanced salt solution
WT	wild type
MOA	mode of action
EMSA	electrophoretic mobility shift assays
ChIP	chromatin immunoprecipitation
SPR	surface plasmon resonance
RT-PCR	reverse transcription-polymerase chain reaction
IPA	Ingenuity Pathway Analysis
RNA-Seq	RNA sequencing
TPO-R	thrombopoietin receptor
EGFRvIII	epidermal growth factor receptor variant III
V-ATPase	vacuolar-type ATPase
FDA	Food and Drug Administration
mTOR	mechanistic (or mammalian) target of rapamycin
HDAC	histone deacetylase
MAPK	mitogen-activated protein kinase
ERK	extracellular signal-regulated kinase

p53	protein 53 or tumor protein 53
MHC1	major histocompatibility complex I
VPS34	vacuolar protein sorting 34
ULK1	unc-51 like autophagy activating kinase 1
ATG4B	autophagy-related 4B
PD-L1	programmed cell death-ligand 1

V. Supplementary References

1. Ronan B*, et al.* (2014) A highly potent and selective Vps34 inhibitor alters vesicle trafficking and autophagy. *Nat Chem Biol* 10(12):1013-1019.
2. Bago R*, et al.* (2014) Characterization of VPS34-IN1, a selective inhibitor of Vps34, reveals that the phosphatidylinositol 3-phosphate-binding SGK3 protein kinase is a downstream target of class III phosphoinositide 3-kinase. *The Biochemical journal* 463(3):413-427.
3. Robke L*, et al.* (2017) Phenotypic Identification of a Novel Autophagy Inhibitor Chemotype Targeting Lipid Kinase VPS34. *Angewandte Chemie* 56(28):8153-8157.
4. Foley DJ*, et al.* (2020) Phenotyping Reveals Targets of a Pseudo-Natural-Product Autophagy Inhibitor. *Angew Chem Int Ed Engl* 59(30):12470-12476.
5. Martin KR*, et al.* (2018) A Potent and Selective ULK1 Inhibitor Suppresses Autophagy and Sensitizes Cancer Cells to Nutrient Stress. *iScience* 8:74-84.
6. Egan DF*, et al.* (2015) Small Molecule Inhibition of the Autophagy Kinase ULK1 and Identification of ULK1 Substrates. *Mol Cell* 59(2):285-297.
7. Pavlinov I, Salkovski M, & Aldrich LN (2020) Beclin 1-ATG14L Protein-Protein Interaction Inhibitor Selectively Inhibits Autophagy through Disruption of VPS34 Complex I. *Journal of the American Chemical Society* 142(18):8174-8182.
8. Qiu Z*, et al.* (2016) Discovery of Fluoromethylketone-Based Peptidomimetics as Covalent ATG4B (Autophagin-1) Inhibitors. *ACS medicinal chemistry letters* 7(8):802-806.
9. Huang SC*, et al.* (2020) Discovery and optimization of pyrazolopyrimidine sulfamates as ATG7 inhibitors. *Bioorganic & medicinal chemistry* 28(19):115681.
10. Laraia L*, et al.* (2019) The cholesterol transfer protein GRAMD1A regulates autophagosome biogenesis. *Nat Chem Biol* 15(7):710-720.
11. Samie M*, et al.* (2013) A TRP channel in the lysosome regulates large particle phagocytosis via focal exocytosis. *Developmental cell* 26(5):511-524.
12. Njomen E & Tepe JJ (2019) Regulation of Autophagic Flux by the 20S Proteasome. *Cell chemical biology* 26(9):1283-1294.e1285.
13. Bowman EJ, Siebers A, & Altendorf K (1988) Bafilomycins: a class of inhibitors of membrane ATPases from microorganisms, animal cells, and plant cells. *Proceedings of the National Academy of Sciences of the United States of America* 85(21):7972-7976.
14. Huss M*, et al.* (2002) Concanamycin A, the specific inhibitor of V-ATPases, binds to the V(o) subunit c. *J Biol Chem* 277(43):40544-40548.
15. Xie XS*, et al.* (2004) Salicylihalamide A inhibits the V0 sector of the V-ATPase through a mechanism distinct from bafilomycin A1. *J Biol Chem* 279(19):19755-19763.
16. Boyd MR*, et al.* (2001) Discovery of a novel antitumor benzolactone enamide class that selectively inhibits mammalian vacuolar-type (H+)-atpases. *The Journal of pharmacology and experimental therapeutics* 297(1):114-120.
17. Sørensen MG, Henriksen K, Neutzsky-Wulff AV, Dziegiel MH, & Karsdal MA (2007) Diphyllin, a novel and naturally potent V-ATPase inhibitor, abrogates acidification of the osteoclastic resorption lacunae and bone resorption. *Journal of bone and mineral research : the official journal of the American Society for Bone and Mineral Research* 22(10):1640-1648.
18. Wang Y*, et al.* (2020) Pharmacological Targeting of Vacuolar H(+)-ATPase via Subunit V1G Combats Multidrug-Resistant Cancer. *Cell chemical biology* 27(11):1359-1370.e1358.
19. Aldrich LN*, et al.* (2015) Discovery of a Small-Molecule Probe for V-ATPase Function. *Journal of the American Chemical Society* 137(16):5563-5568.
20. Mauthe M*, et al.* (2018) Chloroquine inhibits autophagic flux by decreasing autophagosome-lysosome fusion. *Autophagy* 14(8):1435-1455.
21. Laraia L*, et al.* (2017) Discovery of Novel Cinchona-Alkaloid-Inspired Oxazatwistane Autophagy Inhibitors. *Angew Chem Int Ed Engl* 56(8):2145-2150.
22. Laraia L*, et al.* (2020) Image-Based Morphological Profiling Identifies a Lysosomotropic, Iron-Sequestering Autophagy Inhibitor. *Angew Chem Int Ed Engl* 59(14):5721-5729.
23. Shao A*, et al.* (2016) Enhancement of Autophagy by Histone Deacetylase Inhibitor Trichostatin A Ameliorates Neuronal Apoptosis After Subarachnoid Hemorrhage in Rats. *Molecular neurobiology* 53(1):18-27.
24. Renna M*, et al.* (2011) Azithromycin blocks autophagy and may predispose cystic fibrosis patients to mycobacterial infection. *The Journal of clinical investigation* 121(9):3554-3563.

25. Liu Y*, et al.* (2013) Autosis is a Na+,K+-ATPase-regulated form of cell death triggered by autophagy-inducing peptides, starvation, and hypoxia-ischemia. *Proceedings of the National Academy of Sciences of the United States of America* 110(51):20364-20371.
26. Jiang T*, et al.* (2015) Ischemic preconditioning provides neuroprotection by induction of AMP-activated protein kinase-dependent autophagy in a rat model of ischemic stroke. *Molecular neurobiology* 51(1):220-229.
27. Liu N, Shang J, Tian F, Nishi H, & Abe K (2011) In vivo optical imaging for evaluating the efficacy of edaravone after transient cerebral ischemia in mice. *Brain research* 1397:66-75.
28. Cui DR*, et al.* (2013) Propofol prevents cerebral ischemia-triggered autophagy activation and cell death in the rat hippocampus through the NF-κB/p53 signaling pathway. *Neuroscience* 246:117-132.
29. McAfee Q*, et al.* (2012) Autophagy inhibitor Lys05 has single-agent antitumor activity and reproduces the phenotype of a genetic autophagy deficiency. *Proceedings of the National Academy of Sciences of the United States of America* 109(21):8253-8258.
30. Mizumura K*, et al.* (2014) Mitophagy-dependent necroptosis contributes to the pathogenesis of COPD. *The Journal of clinical investigation* 124(9):3987-4003.
31. Zheng Y*, et al.* (2014) Inhibition of autophagy contributes to melatonin-mediated neuroprotection against transient focal cerebral ischemia in rats. *Journal of pharmacological sciences* 124(3):354-364.
32. Petherick KJ*, et al.* (2015) Pharmacological inhibition of ULK1 kinase blocks mammalian target of rapamycin (mTOR)-dependent autophagy. *J Biol Chem* 290(18):11376-11383.
33. Akin D*, et al.* (2014) A novel ATG4B antagonist inhibits autophagy and has a negative impact on osteosarcoma tumors. *Autophagy* 10(11):2021-2035.
34. Zhao H*, et al.* (2013) Role of autophagy in early brain injury after subarachnoid hemorrhage in rats. *Molecular biology reports* 40(2):819-827.
35. Sabatini DM, Erdjument-Bromage H, Lui M, Tempst P, & Snyder SH (1994) RAFT1: a mammalian protein that binds to FKBP12 in a rapamycin-dependent fashion and is homologous to yeast TORs. *Cell* 78(1):35-43.
36. Blommaart EF, Luiken JJ, Blommaart PJ, van Woerkom GM, & Meijer AJ (1995) Phosphorylation of ribosomal protein S6 is inhibitory for autophagy in isolated rat hepatocytes. *J Biol Chem* 270(5):2320-2326.
37. Liu Q*, et al.* (2010) Discovery of 1-(4-(4-propionylpiperazin-1-yl)-3-(trifluoromethyl)phenyl)-9-(quinolin-3-yl)benz o[h][1,6]naphthyridin-2(1H)-one as a highly potent, selective mammalian target of rapamycin (mTOR) inhibitor for the treatment of cancer. *J Med Chem* 53(19):7146-7155.
38. Chresta CM*, et al.* (2010) AZD8055 is a potent, selective, and orally bioavailable ATP-competitive mammalian target of rapamycin kinase inhibitor with in vitro and in vivo antitumor activity. *Cancer research* 70(1):288-298.
39. Chung CY*, et al.* (2019) Covalent targeting of the vacuolar H(+)-ATPase activates autophagy via mTORC1 inhibition. *Nat Chem Biol* 15(8):776-785.
40. Lim CY*, et al.* (2019) ER-lysosome contacts enable cholesterol sensing by mTORC1 and drive aberrant growth signalling in Niemann-Pick type C. *Nature cell biology* 21(10):1206-1218.
41. Chiang WC*, et al.* (2018) High-Throughput Screens To Identify Autophagy Inducers That Function by Disrupting Beclin 1/Bcl-2 Binding. *ACS chemical biology* 13(8):2247-2260.
42. Chen CC*, et al.* (2014) A small molecule restores function to TRPML1 mutant isoforms responsible for mucolipidosis type IV. *Nature communications* 5:4681.
43. Shoji-Kawata S*, et al.* (2013) Identification of a candidate therapeutic autophagy-inducing peptide. *Nature* 494(7436):201-206.
44. Sarkar S*, et al.* (2007) Small molecules enhance autophagy and reduce toxicity in Huntington's disease models. *Nat Chem Biol* 3(6):331-338.
45. Sarkar S*, et al.* (2005) Lithium induces autophagy by inhibiting inositol monophosphatase. *The Journal of cell biology* 170(7):1101-1111.
46. Siddiqi FH*, et al.* (2019) Felodipine induces autophagy in mouse brains with pharmacokinetics amenable to repurposing. *Nature communications* 10(1):1817.
47. Rusilowicz-Jones EV*, et al.* (2020) USP30 sets a trigger threshold for PINK1-PARKIN amplification of mitochondrial ubiquitylation. *Life science alliance* 3(8).
48. Cool B*, et al.* (2006) Identification and characterization of a small molecule AMPK activator that treats key components of type 2 diabetes and the metabolic syndrome. *Cell metabolism* 3(6):403-416.
49. Kim JJ*, et al.* (2012) Host cell autophagy activated by antibiotics is required for their effective antimycobacterial drug action. *Cell host & microbe* 11(5):457-468.
50. Cinque L*, et al.* (2015) FGF signalling regulates bone growth through autophagy. *Nature* 528(7581):272-275.

51. Kuo SY*, et al.* (2015) Small-molecule enhancers of autophagy modulate cellular disease phenotypes suggested by human genetics. *Proceedings of the National Academy of Sciences of the United States of America* 112(31):E4281-4287.
52. Morselli E*, et al.* (2010) Caloric restriction and resveratrol promote longevity through the Sirtuin-1-dependent induction of autophagy. *Cell death & disease* 1(1):e10.
53. Lee S*, et al.* (2014) Carbon monoxide confers protection in sepsis by enhancing beclin 1-dependent autophagy and phagocytosis. *Antioxidants & redox signaling* 20(3):432-442.
54. Sala-Mercado JA*, et al.* (2010) Profound cardioprotection with chloramphenicol succinate in the swine model of myocardial ischemia-reperfusion injury. *Circulation* 122(11 Suppl):S179-184.
55. Matsuda C*, et al.* (2007) Therapeutic effect of a new immunosuppressive agent, everolimus, on interleukin-10 gene-deficient mice with colitis. *Clinical and experimental immunology* 148(2):348-359.
56. Sun L*, et al.* (2015) Hydrogen sulfide reduces serum triglyceride by activating liver autophagy via the AMPK-mTOR pathway. *American journal of physiology. Endocrinology and metabolism* 309(11):E925-935.
57. Pietrocola F*, et al.* (2016) Caloric Restriction Mimetics Enhance Anticancer Immunosurveillance. *Cancer cell* 30(1):147-160.
58. Gutierrez MG*, et al.* (2004) Autophagy is a defense mechanism inhibiting BCG and Mycobacterium tuberculosis survival in infected macrophages. *Cell* 119(6):753-766.
59. Li XZ*, et al.* (2013) Therapeutic effects of valproate combined with lithium carbonate on MPTP-induced parkinsonism in mice: possible mediation through enhanced autophagy. *The International journal of neuroscience* 123(2):73-79.
60. Chen J*, et al.* (2014) Melatonin-enhanced autophagy protects against neural apoptosis via a mitochondrial pathway in early brain injury following a subarachnoid hemorrhage. *Journal of pineal research* 56(1):12-19.
61. Song YM*, et al.* (2015) Metformin alleviates hepatosteatosis by restoring SIRT1-mediated autophagy induction via an AMP-activated protein kinase-independent pathway. *Autophagy* 11(1):46-59.
62. He C*, et al.* (2012) Exercise-induced BCL2-regulated autophagy is required for muscle glucose homeostasis. *Nature* 481(7382):511-515.
63. Vingtdeux V*, et al.* (2010) AMP-activated protein kinase signaling activation by resveratrol modulates amyloid-beta peptide metabolism. *J Biol Chem* 285(12):9100-9113.
64. Zhou Y*, et al.* (2016) Retinoic Acid Prevents Disruption of Blood-Spinal Cord Barrier by Inducing Autophagic Flux After Spinal Cord Injury. *Neurochemical research* 41(4):813-825.
65. Eisenberg T*, et al.* (2009) Induction of autophagy by spermidine promotes longevity. *Nature cell biology* 11(11):1305-1314.
66. Ravikumar B*, et al.* (2004) Inhibition of mTOR induces autophagy and reduces toxicity of polyglutamine expansions in fly and mouse models of Huntington disease. *Nature genetics* 36(6):585-595.
67. Castillo K*, et al.* (2013) Trehalose delays the progression of amyotrophic lateral sclerosis by enhancing autophagy in motoneurons. *Autophagy* 9(9):1308-1320.
68. Xie M*, et al.* (2014) Histone deacetylase inhibition blunts ischemia/reperfusion injury by inducing cardiomyocyte autophagy. *Circulation* 129(10):1139-1151.
69. Sardiello M*, et al.* (2009) A gene network regulating lysosomal biogenesis and function. *Science* 325(5939):473-477.
70. Ianevski A, He L, Aittokallio T, & Tang J (2017) SynergyFinder: a web application for analyzing drug combination dose-response matrix data. *Bioinformatics* 33(15):2413-2415.
71. Zhang WZ*, et al.* (2019) The protein complex crystallography beamline (BL19U1) at the Shanghai Synchrotron Radiation Facility. *Nuclear Science And Techniques* 30(11).
72. Kabsch W (2010) Integration, scaling, space-group assignment and post-refinement. *Acta Crystallogr D Biol Crystallogr* 66(Pt 2):133-144.
73. Collaborative Computational Project N (1994) The CCP4 suite: programs for protein crystallography. *Acta crystallographica. Section D, Biological crystallography* 50(Pt 5):760-763.
74. Emsley P & Cowtan K (2004) Coot: model-building tools for molecular graphics. *Acta crystallographica. Section D, Biological crystallography* 60(Pt 12 Pt 1):2126-2132.
75. Adams PD, Mustyakimov M, Afonine PV, & Langan P (2009) Generalized X-ray and neutron crystallographic analysis: more accurate and complete structures for biological macromolecules. *Acta crystallographica. Section D, Biological crystallography* 65(Pt 6):567-573.